IEEE Access
Multidisciplinary | Rapid Review | Open Access Journal

Received 27 July 2023, accepted 9 August 2023, date of publication 17 August 2023, date of current version 25 August 2023.

Digital Object Identifier 10.1109/ACCESS.2023.3305958

RESEARCH ARTICLE

High Impedance Fault Detection on Microgrids Considering the Impact of VSC Based Generation

VITOR FERNANDO COUTO AND MIGUEL MORETO
Department of Electrical and Electronics Engineering, Federal University of Santa Catarina, Florianópolis 88040-900, Brazil
Corresponding author: Vitor Fernando Couto (vitorfernandocouto@gmail.com)

This work was supported in part by Coordenação de AperfeiÇoamento de Pessoal de Nível Superior-Brasil (CAPES) under Grant 001.

ABSTRACT This paper presents an evaluation of the impacts of simulation models for high impedance faults detection in microgrids with distributed generators interfaced by voltage source converters. Detailed simulation models are used to consider the high frequency switching of power electronics and, consequently, the associated harmonic distortions. Thus, for systems with a higher degradation of the current sine waveform, the high impedance fault characteristics such as nonlinearity, asymmetry, and randomness may remain hidden, compromising the performance of some existing detection techniques. Such models are not commonly used in the high impedance fault detection literature. To evaluate the impact of the simulation model's complexity, a pretrained deep convolutional neural networks on the imageNet database is adapted to classify current waveform based on a time-frequency representation image. The proposed method is designed and tested using a microgrid model based on the CIGRE European medium voltage distribution network benchmark. The simulation data set considers microgrid operating in islanded and connected manner, radial and ring topology, with transients at different locations of the network. The results indicate that high impedance fault detection methods for microgrid with voltage source converters generators need to be designed using detailed simulation models to achieve better accuracy, and the proposed classifier presented accurate and robust high impedance fault detection.

INDEX TERMS High impedance fault, microgrid, simulation models, transfer learning, voltage sourced converter.

I. INTRODUCTION

The concern with climate change, the greenhouse effect, and the pursuit for independence from fossil fuels has led to a major transformation of electrical power systems. In recent years, renewable distributed generation (DG) has been inserted into the distribution network to meet the ever-increasing demand for electricity locally [1]. This trend is expected to be stronger in future grids with a higher degree of renewable energy sources that are usually interfaced using voltage source converters (VSCs).

In this environment, microgrid (MG) have emerged, facilitating the incorporation of DG power sources. Such a concept can result in greater reliability to the electricity supply since they can operate connected or islanded from the main grid. Some of the concerns with protection systems in MG include the possibility of reversible power flows and different short-circuit levels depending on the operation mode. In addition, the variations associated with generation, loads, and configuration lead to challenges to be overcome [2].

Traditional protection schemes need to be adapted to these new characteristics of MG. Among the problems to be overcome, high impedance fault (HIF) provides various complex issues for the utility industry, as conventional overcurrent relays fail to detect HIFs due to the low current levels. This type of fault can occur when an energized conductor touches the surface with a high impedance, such as vegetation near overhead distribution lines or when the conductor falls to the ground. These situations expose electrical system equipment, private properties, and especially human lives to risk [3].

For this reason, more efficient detection methods were proposed, most of them based on tracking voltage and current distortions due to the HIF. This protection issue in distribution systems networks is not an outdated problem [4] and becomes

The associate editor coordinating the review of this manuscript and approving it for publication was Hazlie Mokhlis.

even more challenging in a MG with a high penetration of generators interfaced by VSC [5].

An extensive review of HIF detection methods was covered in [4]. Distortions due to nonlinearity of voltage and current, asymmetry between positive and negative semi-cycles, nonstationary current and, randomness arise from HIF. Detection methods typically use signal processing techniques to identify these features within voltage and current signals in a harmonic-free environment. Nevertheless, in MG characterized by a substantial deployment of VSC generators, a notable level of distortion arises, potentially impeding the effectiveness of detection algorithms. In addition, switching transients have HIF-like characteristics, such as capacitor bank connection and large single-phase load switches, which can lead to false detections.

There are some studies in the technical literature that propose solutions to detect HIF in systems with DG, as in [6] and [7]. Despite the consideration of DG and HIFs, the test systems utilized were free of harmonic distortions. Such circumstances are improbable at present, but the prognosis suggests a worsening situation in the future for distribution systems, particularly in MGs. In the existing literature, the considered distortions [5], [8], [9], [10], [11] primarily stemmed from the utilization of detailed simulation models for VSC generators. Nonetheless, the literature fails to encompass MG scenarios involving island operation and ring topology.

Certain papers have previously addressed the HIF problem in MGs, but without providing specific details regarding the representation of distributed generation, as observed in [12], [13], [14], and [15].

There are methods for detecting HIF in MG that take into account the application of comprehensive simulation models for VSC-based generation. In [16], a protection scheme for microgrids capable of detecting HIF was presented. The test system comprised an IEC model test microgrid incorporating a DFIG-based wind farm, an inverter-based DG wind farm, and two synchronous DGs. However, the authors did not examine this aspect in their results.

A long short-term memory (LSTM) based protection scheme was proposed to detect HIF in hybrid MG [17]. The PV DG consider a statistical modelling for solar irradiance intermittency, combining Gaussian distribution function and meteorological data. Although the DG was not a source of harmonic intrusion in the simulation data, the approach's immunity to it was evaluated separately for nonlinear loads and Gaussian noise. The real-world applicability of this approach may be affected since Gaussian noise cannot accurately recreate the dynamics of PV DG in transient states, particularly in high penetration VSC DG and MG islanded operation. This was also the case for the papers [18], [19].

Moreover, in [20] the LSTM was used to classify HIF with three-phase current signal. The method achieve overall classification accuracy of 91.21% and outperforms well-known classifiers in tests performed. This approach consider PV DG with detailed model in a distribution network.

The authors of [21] and [22] proposed HIF protection strategies for MG while taking VSC DG into account, but they discovered performance deterioration for the island operation mode. Detection and classification of MG faults in [23] take into account radial and meshed topology and also the mode of operation. Additionally, in [24], a protection strategy for MG was presented, considering HIF and thresholds were established for residual voltage and current. However, to achieve selectivity in the HIF detection logic, a delay of at least 0.5 seconds had to be included.

Based on the aforementioned studies, a small number of works took DG into account using detailed models. Even among those that did, they did not examine its impact on the classification problem. These findings highlight the need for further investigation into this subject. Thus, this paper intends to discuss the impact of detailed simulation models on HIF detection in MG systems and also proposes an effective classification method. The results were compared with a recent method from the literature.

The proposed detection method uses as input current signals converted into RGB images for a Deep Neural Network (DNN) classifier. This approach has the advantage of being independent of prior knowledge and human intervention in feature extraction. The goal is to show detailed simulation models result in more realistic data, providing a challenging condition for HIF detection methods. In summary, the contributions of this paper can be stated as follows:

- Proposition of a novel HIF detection method using image classification techniques. The approach uses VSC simulation models to accurately capture the effects of switching frequency and dynamic VSC generator characteristics.
- The development of a methodology to identify HIF using transfer learning from 2-dimensional DNN features trained on ImageNet [25].
- The transformation of a time series signal into an RGB image by means of a Continuous Wavelet Transform (CWT).
- Variations in the MG's modes of operation (islanded or connected) and topology (ring of radial) are taken into account during HIF detection.
- Comparative evaluation of numerical results with other existing approaches [15], [16], [17], [18], [20].
- Evaluation with five performance indexes and compare the results with similar method [20] for the same database.
- Noise resilience test adding current signals white Gaussian noise of varying levels (0 dB < SNR < 30 dB).
- Tests are conducted with three different HIF models to evaluate the method's ability to recognize HIF with different characteristics for which it has not been trained.

The rest of this paper is organized as follows. Section II explains MG features and VSC generators simulation models. HIF features and simulation models used are described in Section III. Section IV contains the proposed methodology and data set description. Section V provides the classification

test results and analysis. At the final Section VI presents the conclusions and further development intentions.

II. MICROGRID TOPOLOGY, LOADS AND GENERATORS

In MGs, it is possible to have reversible power flows, different levels of short-circuit for the islanded and connected modes, and the presence of VSC generators behave differently from synchronous generators. All these features require different protection than traditional distribution systems [26].

In this paper, the MG test system has simulation models that consider the VSC switching circuits that reproduce the associated harmonic distortions. These distortions can impact the effectiveness of HIF detection algorithms, causing misclassification or lack of sensibility [22], [27], [28].

A. MICROGRID

The system used is an adaptation of one of the test systems presented in [29] by CIGRE's commission C6 (Distribution and Distributed Generation Systems). This system is called *Topology of European MV Distribution Network Benchmark*, and was chosen among the two that operate at medium voltage (European and North American). The MG structure has two feeders, but only feeder 1 is considered in this work. System operation settings were changed from 20kV-50Hz to 25kV-60Hz. The loads are balanced, all the lines are overhead and three-phase with non-insulated aluminum conductors. The MG single line diagram is shown in the Fig. 1.

In [29] it is stated that grounding is a matter of regional preferences, being the European distribution networks typically isolated or grounded by impedance. In this work it is considered a MG with a grounding zig-zag transformer (GT), connected between bus 1 and T1, to create a low-impedance path for zero sequence currents, while being high impedance for positive and negative sequence currents. There are three switches, S1 is the Common Connection Point (PCC) that allows the MG to operate in an isolated or connected mode. When tie switches S2 and S3 are closed, the MG has a loop configuration, and when both are opened, the system becomes radial.

The distributed generation sources are included using detailed models, that represent static VSC power converters. The DG consists of three solar power plants, one wind power plant and one synchronous generator. This synchronous generator acts as a synchronous reference in islanded connection mode, responsible for power balance, modeled as a three-phase source with an internal R-L impedance. The other generators controls are set to extract maximum power from the available primary energy.

B. PHOTOVOLTAIC GENERATOR

The MG contains three photovoltaic plants of 100kWp each, connected to the network by 100kVA, 25kV/600V (D11Yg) transformers. It can be seen in Fig. 2, the plants have two converters, the DC-DC and the VSC. The DC-DC boost converter regulates the output voltage of photovoltaic panels, which varies according to the intensity of solar irradiance

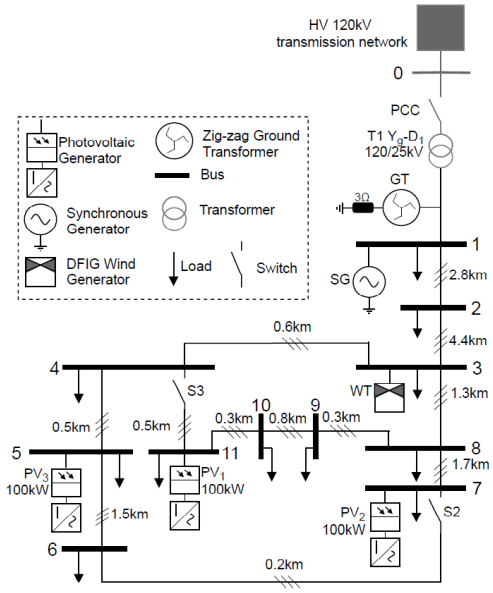

FIGURE 1. Single line diagram of the microgrid based on CIGRE's European MV distribution network benchmark.

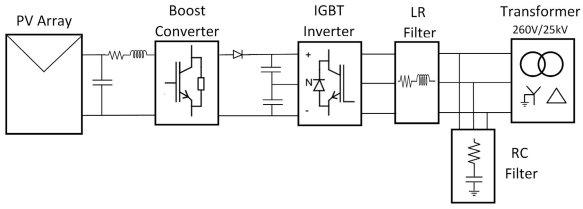

FIGURE 2. Simulation model of the PV generator.

(273 V_{dc} at maximum power) to 500 V_{dc}. The VSC converts this continuous voltage to 260V_{ac}, operating with a unit power factor. It is also considered an RC filter to mitigate the harmonic distortions.

The plant has an MPPT (*Maximum Power Point Tracking*) control that adjusts the operating point for the highest energy output. The simulations are performed with a temperature of 45°C and an irradiance of 1000 W/m^2. The remaining parameters of this PV farm are the same as the one in [30].

C. WIND GENERATOR

The wind power plant is based on 1.5 MW Double-Fed Induction Generators (DFIG). The plant is composed of six generators, with an output voltage of 575V_{ac}, connected to Bus 3 of the MG through a 25kV/575V (D11yg) 9MW transformer.

Fig. 3 shows the scheme for one of these generators, where the implemented model includes a representation of the IGBT-based converters (1620 Hz and 2700 Hz switching frequencies). The armature winding (or stator) is connected to the network, and the field winding (rotor) is connected to VSC converters. The converters are called RSC (Rotor Side Converter) and LSC (Line Side Converter) and allow the frequency of the field winding to be adjustable. This way, the generator can operate at variable speeds with increased efficiency.

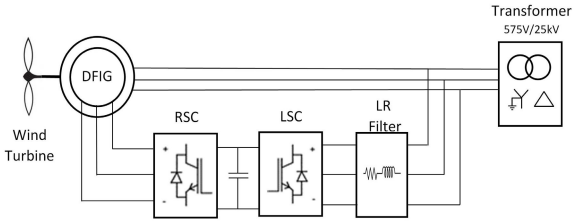

FIGURE 3. Simulation model of the DFIG wind generator and its associated power converters.

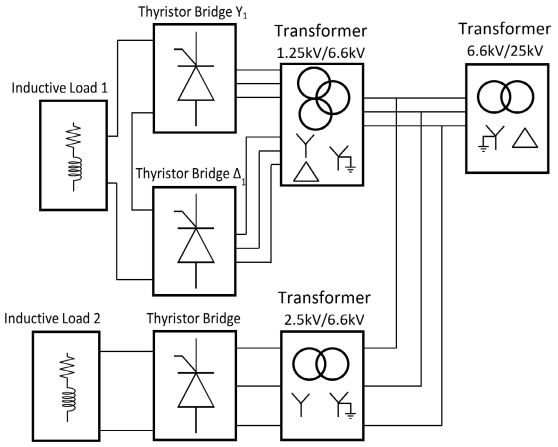

FIGURE 4. Simulation model of the non-linear load with two thyristor rectifiers.

In the simulations, the plant operates with a constant wind at 15 m/s and the reactive power is set to 0 MVAr. The same model was used in [21] and [23].

D. NON-LINEAR LOAD

It was not something new that certain loads share characteristics with HIF, which can result in false triggers. These loads, such as arc welders, furnaces, computers, and other non-linear applications, produce harmonic distortions [31]. Thus, it is necessary to test the ability of HIF detection methods to distinguish between the fault and switching of this type of load. In [27] and [32], Soheili et al had proposed methods for HIF detection, taking into account the presence of non-linear loads. In this paper, a detailed Matlab/Simulink model of a three-phase six-pulse bridge thyristor rectifier is used as a building block for a non-linear load as shown in Fig. 4. Load 1 is supplied by two six-pulse bridges connected in series, with their AC connections in a transformer with two secondary windings (one wye, one delta). Load 2 is supplied by a single six-pulse bridge. The combination of the two loads results in a consumption of 500 kW 800kVAr with 17% THDi.

III. HIGH IMPEDANCE FAULTS

The main detectable characteristics of HIFs are due to the formation of an electric arc. This arc generates a distorted electrical current, alternating between conduction and no conduction cycles. The voltage threshold to dielectric rupture is different for positive and negative voltages, resulting in asymmetry in voltage and current waveforms. The electrical current resulting from this type of fault has a frequency spectrum that varies over time. In addition, current magnitude and conduction intervals are random events. This relationship between voltage and current is non-linear and generates harmonic components [33].

The majority of HIF detection techniques employ electrical current measurements, as illustrated in [3] and [4]. There are also some methods using a combination of voltage and current or magnetic fields. To classify the event, characteristics are taken from the collected voltage and/or current data. These characteristics may be in the time domain, frequency domain, time-scale domain, or time-frequency domain. The physical phenomenon of HIF very often involves electrical arcing, making the electrical current random and unpredictable. A variety of current waveforms are produced by environmental factors including humidity and the kind of contact surface.

The development of HIF detection techniques with satisfactory performance is closely related to the quality of the database used. This data can be obtained through field tests. It is necessary to perform these field tests, special equipment and skilled labor are required. The characteristics of these data tend to be more specific to the distribution system tested, making them difficult to generalize and use in other systems [34]. Another option is the use of simulation models to obtain this data. With a few adaptations, it is possible to apply HIF to different systems and test them for a wide variety of events. The HIF waveforms obtained from simulation models were equivalent to those from field tests, confirming their validity [7].

This paper uses three different HIF simulation models to create the database for the proposed detection method. These models were variations of Emanuel's HIF model [33] that use a combination of electrical elements like voltage sources, diodes, inductances, and resistances to reproduce the HIF characteristics. The Emanuel model was based on laboratory experiments, field measurements, and theoretical calculations. Since then, a number of further articles have proposed refining and adapting this model to better represent this physical phenomenon [4].

The source-diode-resistance HIF model, shown in Fig. 5 (a), has tuned parameters to suit the system voltage and is connected between phase (V_{ph}) and ground. In this model, the positive branch (R_P) and (V_P) have smaller values relative to the negative branch (R_N) and (V_N) to reproduce the half-cycle asymmetry and intermediate arc extinction observed in the HIF waveforms. In this circuit, current flows to ground when the instantaneous value $V_{ph} > V_P$, reverse when $V_{ph} > V_N$ and if $V_N < V_{ph} < V_P$ there is no fault current.

In this paper, three different HIF models (named Model I, Model II and Model III) are employed in Matlab/Simulink for multiple simulations. The inclusion of three different models helps build a database that includes all of the HIFs' features while preventing the proposed method from becoming overfit.

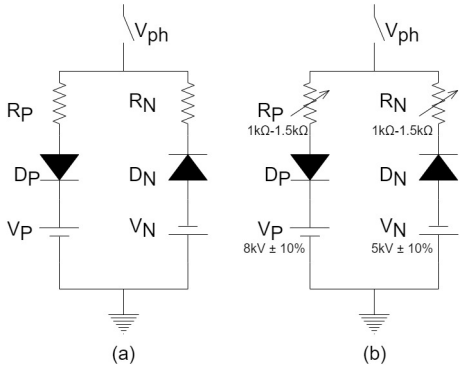

FIGURE 5. Emanuel type of HIF simulation circuits: (a) model I [35] and (b) model III [7].

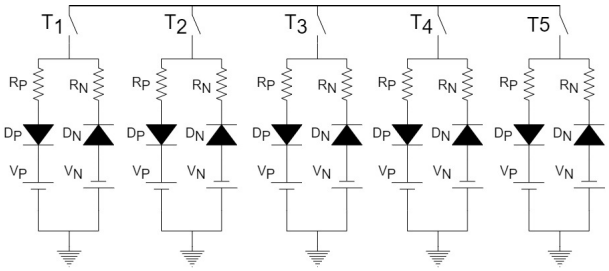

FIGURE 6. Circuit of HIF simulation model II [37].

A. HIF MODEL I

The HIF I model was based on Emanuel's model [33], where inductance and resistance have been replaced by resistors of unequal values to reproduce the asymmetry in the current waveform. This model reproduces low frequency phenomena typical of an arcing fault involving sandy soil. The circuit is shown in Fig. 5 (a), and ten sets of typical values for DC sources and resistors were shown in [35].

This model, although being frequently used in the development of detection techniques, is unable to recreate the build-up and shoulder characteristics of an HIF [36].

B. HIF MODEL II

The HIF model II was based on the Emanuel arc model but used six arc models in parallel, as shown in Fig. 6, to improve HIF simulation. Each one of the six arc circuit refers to the occurrence of an electric arc, and their values of resistances, DC-sources, and switching time for five different fault types were detailed in [37]. These values were adjusted to fit the waveforms obtained through real-world testing. The authors proposed one HIF model for each of five different surfaces, with a variation in the maximum amplitude of the fault current between 9 and 90 A.

This model reproduces the first eight cycles of HIF current with some characteristics, such as asymmetry and nonlinearity of the HIF, and all frequency components up to 12 kHz.

C. HIF MODEL III

The HIF model III is similar to model I, but the values for resistance and DC sources vary randomly and independently every 0.1 ms [7]. The model is also simple and gets all

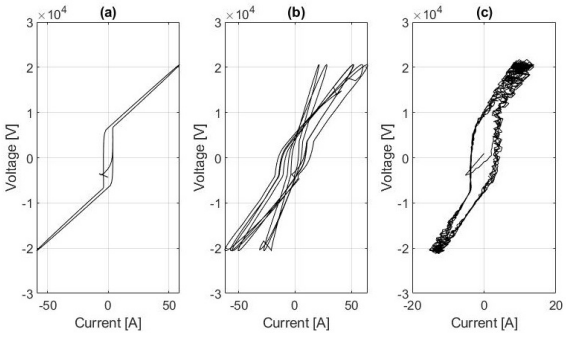

FIGURE 7. V-I characteristics of HIF (a) model I (b) model II (c) model III.

the characteristics of HIF current, such as: intermittence, asymmetry, buildup, shoulder, randomness, and nonlinearity. In the actual settings of the benchmark MG employed in this paper, V_P and V_N vary randomly pm 10% around 8 kV and 5 kV independently every 0.1 ms. Also, the two independently and randomly changing resistors R_P and R_N are varying between 1000 Ω and 1500 Ω, at a rate of 0.1 ms as well. The circuit of HIF model III is presented in Fig. 5 (b).

Fig. 7 depicts the V-I characteristics of the HIF models. The first graphic, Fig. 7 (a), represents HIF model I with settings $V_N = 6155V$, $V_P = 6180V$, $R_N = 245\Omega$ and $V_N = 245\Omega$. In Fig. 7 (b) the characteristics are to the HIF model II state 2. The third graphic, Fig. 7 (c), show HIF model III. The total harmonic distortion for these examples of HIF is 20%, 8% and 22% respectively.

IV. THE PROPOSED CLASSIFIER AND DATA SETS

HIF detection is not a simple task, and as can be seen in the literature, there are several papers that propose to solve this problem with different approaches [4]. In this work, some features extracted from measurements of the test system have been evaluated, and the simply setting thresholds was not able to determine the occurrence of a HIF. Therefore, a state-of-the-art pattern recognition technique is used to evaluate the impact that simulation model complexity has on HIF detection method's performance. This technique is described below.

A. CLASSIFICATION FEATURES AND TRAINING METHOD

In [38] the detection of HIF in the distribution network used a time-frequency-based method. The algorithm performs five steps to extract a set of minimally relevant features from the measured current to detect HIF. These tasks are complex and involve the creation of 2D matrix with time-frequency distributions, feature dimensionality reduction (PCA - Principal Component Analysis), and classification by support vector machine (SVM).

The detection method proposed here also uses the time-frequency characteristics of the current but takes fewer steps. From the three-phase current measurements the instantaneous residual current is calculated ($I_R(t) = I_a(t) + I_c(t) + I_c(t)$) [39]. Applying Continuous Wavelet Transform (CWT) results in a RGB image which is the input data of a pretrained DNN.

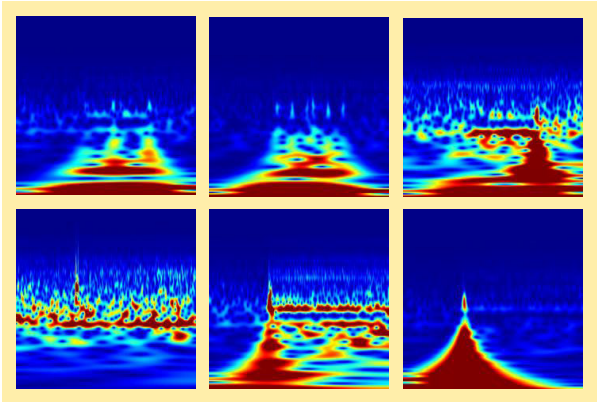

FIGURE 8. Examples of scalograms. The top images correspond to 3 HIF images while the bottom ones are obtained from other switching events.

The DNN has an architecture that learns from data, eliminating the need for feature extraction [40]. Thus, a technique called transfer learning was used reducing the need and effort for training data collection. Also, transfer learning is applied to take advantage of the existing neural networks, it has been trained on large data sets, such as ImageNet [25] for image classification. The selection of DNN represents a trade-off between three qualities: accuracy, speed, and size. The DNNs VGG19, Squeezenet, GoogleNet, and AlexNet were examined and tested. SqueezeNet [41] was chosen due to its improved performance and compact size, which facilitates implementation. The transfer learning technique for HIF detection was used in [42], [43], and [44] but not with image classification.

The first and second steps is the calculation and conversion of residual current I_R into a scalogram image, which is the absolute value of the CWT coefficients of a signal. Each of the simulations performed has a corresponding RGB image of size 227-by-227-by-3, where 3 is the number of color channels. These images form the data sets to train and test the deep CNN. These images are time-frequency representations of I_R current, and some examples are shown in Fig. 8.

The third step consists of training the DNN to recognize HIF. During the transfer learning process, some of the 18 layers of the SqueezeNet architecture are replaced with new ones. The first layers identify common image characteristics (spots, edges, and colors), the last layers focus on specific characteristics to distinguish classes. The 'drop9' layer, which prevents overfitting, is replaced with a dropout layer of probability 0.6. Also, the 'conv10' last learnable layer is replaced by a new convolutional layer with two filters that are the number of classes in the data set (HIF and nonHIF). To finish the adjustment, the classification layer is replaced by a new one without class labels. The labels will come from the new training data set. The classification process is presented in Fig. 9.

B. DATABASE

A Simulink/MatLab model of the MG test system was used to collect the signal I_R in bus 3, with 15.36kHz sampling

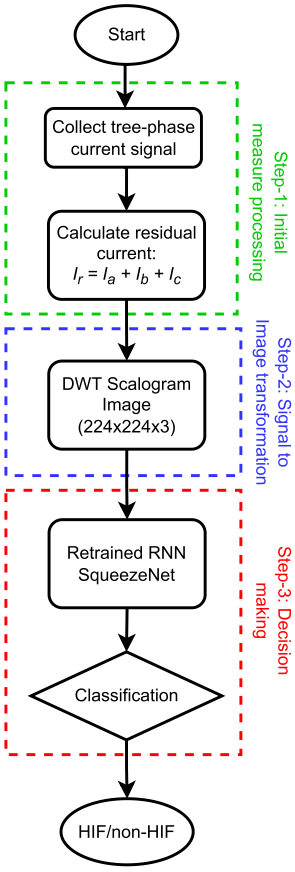

FIGURE 9. Flowchart of the Proposed method.

frequency, for HIF and nonHIF cases. The simulation model is discretized at 5 microseconds time step, due to detailed representation of the VSC converters with switching frequencies of 5kHz (PV) and 2.7kHz (DFIG). The same time step and sampling frequency was used in the simulations with simplified models.

All HIF simulations models were presented in section III.

Others power system switching transients were simulated. These transients share some characteristic with HIF, such as the high-frequency components of load and capacitor switching, and the low frequency components and asymmetry present in transformer inrush currents [3].

All simulations last for 2 seconds. During the first 0.5 seconds the system stabilizes in the steady state condition. Thus, only the final 1.5 seconds were considered to obtain the residual current (I_R) scalogram images. Simulations of training data set are listed below. All simulated transients considered 100%, 80% and 60% MG loading in all combinations of topology (ring or radial) and operating mode (connected or islanded).

1) High impedance faults: intermittent, with and without interruption;
2) Capacitor switching: 600 kVar, 400 kVar and 300 kVar;
3) Transformer switching: switching on and off with 10% and 30% loads;

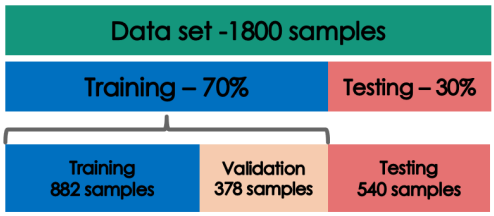

FIGURE 10. Structure of the dataset formed through MatLab/Simulink simulation.

4) Linear load switching: single-phase, two-phase and three-phase connected in delta and wye;
5) Non-linear load switching: as shown in section II-D;
6) Three-phase line switching: combination of S2 and S3 opening and closing, shown in Fig 1;
7) No transient: All MG operation mode and topology combinations with no transient.

These combination results in 1800 (900 HIF and 900 non-HIF) different simulation conditions, as shown in Fig. 10, and two training data set are assembled. The first training set have 1260 images considering DGs with detailed model of the VSC generators. The classifier trained with this data set is referred to as the Detailed Classifier. In the second data set, the detailed models for the DG's are replaced by three-phase source blocks available in MATLAB/Simulink. They are specified to delivering the same active and reactive power as DG's detailed models. The Simple Classifier is derived from this last training data set. SqueezeNet training data set is divided into 70% for training and 30% for validation.

Another data set, with different transient parameters from training, is created to test the performance of the Detailed and Simple classifiers. This test data set has 540 simulation (270 HIF and 270 nonHIF) only with DG's detailed models.

The data sets utilized for testing and training are different. To prevent bias due to the small number of examples, the data for training and testing are manually divided in 70% and 30%, respectively. For the training process, this data is randomly split into training and validation, in a 70/30 ratio, as seen in Fig. 10.

The data sets for training and testing are organized to perform five different tests. To ensure a proper evaluation of the proposed classifier, performance indexes are selected for use.

C. PERFORMANCE EVALUATION

Due to the complexity of the HIF phenomenon and its detection techniques, a complete set of criteria is needed for their evaluation. While tripping the power system due to the HIF guarantees public safety, it would also disconnect vital loads such as traffic lights, elevators, and hospitals. Thus, two criteria, safety and sensibility, are suggested for utilities to use when performing a risk analysis on this tradeoff. The complexity of HIF detection methods necessitates the use of additional indices [3] to assess their efficacy.

Five evaluation indexes derived from the confusion matrix will be utilized. Confusion matrix is a two-by-two matrix defined as:

$$C_m = \begin{bmatrix} DF & ND \\ MF & HC \end{bmatrix} \tag{1}$$

where in the case of detection algorithms, number DF shows the number of right detection of the HIFs, HC demonstrates number of right decision of healthy conditions, MF is number of healthy condition that mistakenly classified as HIFs and finally ND shows the number of HIFs that were not detected [38]. The aim is to achieve the highest values of the five reliability indexes listed below.

- Accuracy: it is the amount of correct detections in relation to the overall number of cases. It emphasizes the Overall precision of the method.

$$AC = \frac{DF + HC}{DF + ND + HC + MF} \tag{2}$$

- Dependability: this index can be expressed as the ratio of the number of identified faults to the actual number of faults. Dependability is defined as faulty state detection precision.

$$DP = \frac{DF}{DF + ND} \tag{3}$$

- Security: it demonstrates the technique's capability to recognize the HIF only when it is present and not trip for nonHIF conditions. It represents the healthy state detection precision.

$$SC = \frac{HC}{HC + MF} \tag{4}$$

- Safety: this index takes into account the method's capacity to isolate faults that pose a risk to the general public, such as HIF in a congested area, assuring that faults are not confused with nonHIF. The number of correctly predicted nonHIF divided by the total number of nonHIF determine this criterion.

$$SF = \frac{HC}{ND + HC} \tag{5}$$

- Sensibility: this index can be defined as the percentage of correctly predicted faults over the total number of predicted faults. Emphasizing the danger of tripping sensitive loads.

$$SN = \frac{DF}{DF + MF} \tag{6}$$

D. COMPARATIVE EVALUATION

In addition to the evaluation indexes, the results are compared with state-of-the-art HIF detection approaches, shown in Table 1. The rates of Proposed approach were slightly lower than those in [17], although this method requires seven currents measurement points. The [15], [18], [20] approaches only employ one point with currents measurement, similar to Proposed method, but for [16], ten voltages and currents measurement points were needed, as presented in Table 2.

The islanded operation mode of the test system was not taken into account in [15], [16], [17], [18], and [20] does

TABLE 1. Comparative evaluation of performance indexes.

Methods	accuracy	dependability	security	safety	sensibility
[15]	99.23%	99.17%	100%	90.91%	100%
[16]	91.60%	-	-	-	-
[17]	99.66%	99.73%	99.29%	-	-
[18]	99.35%	99.35%	100%	89.55%	100%
[20]	91.21%	92.42%	90.63%	95.87%	83.56%
Proposed	99.65%	99.30%	100%	99.30%	100%

TABLE 2. Data set information.

Methods	Test HIF/nonHIF	Train HIF/nonHIF	Measuring Points and Type
[15]	120 / 10	- / -	1 Current
[16]	- / -	- / -	10 Currents and Voltages
[17]	14,817 / 15,805	34,575 / 36,879	7 Currents
[18]	928 / 54	97 / 6	1 Current
[20]	66 / 128	706 / 264	1 Current
Proposed	270 / 270	900 / 360	1 Current

not take noise into account. The test data sets also contain a significant class imbalance, with samples in [15] consisting of 120 HIF and 10 nonHIF, in [18] consisting of 928 HIF and 54 nonHIF, and in [20] consisting of 66 HIF and 128 nonHIF, shown in Table 2. Since the evaluation index for the compared approaches have fairly similar values, all the factors mentioned above should be taken into account.

The details regarding the input data type and sample sizes for the training and testing data sets can be found in Table 2. In [16] the number of samples for testing is not presented.

The HIF detection technique presented in [20] are select to classify the same test data set used in the Proposed method. This work was based on simulations with nonfault (normal operation, capacitor switching, load switching, transformer inrush current) and fault (HIF, symmetrical and unsymmetrical fault) in IEEE 13-bus distribution system with 300 kW PV DGs modeled in MATLAB/Simulink. The detection technique implemented a deep learning method of RNN based LSTM with feature extraction using DWT analysis. The three-phase current signal was processed using db4 mother wavelet to extract each phase's energy value characteristics for training and testing the classifiers.

The authors achieved classification accuracy of 91.21% with a success rate of 92.41% in identifying HIF in the simulations performed. This method [20], using LSTM, follows the same rule for the training data as the SqueezeNet, resulting in the Detailed Method [20] and Simple Method [20] classifiers.

V. CLASSIFICATION TESTS, RESULTS AND ANALYSIS

Five test scenarios were established in order to determine the efficacy of the proposed HIF detection approach. The complete database is used in the initial test. The capacity to recognize model II and III HIF is assessed in the second and third tests, respectively. The performance regarding differentiating between non-linear load and HIF is analyzed in the fourth test. The ability to not identify switching on MG transmission lines as HIF is tested in the fifth and final test.

The results are shown in the same figure for the two Detailed SqueezeNet and Method [20] and for the two

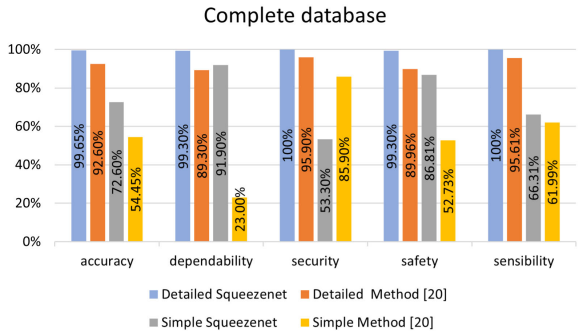

FIGURE 11. Classification performance for the complete data set test.

Simple SqueezeNet and Method [20] classifiers. All tests were performed on simulation data with detailed DG models, thus reproducing a more realistic simulation scenario.

A. CLASSIFICATION TESTS FOR COMPLETE DATA SET

The complete data set comprises a total of 630 cases from each of the three HIF models and 630 non-HIF cases. The latter corresponds to 245 cases of the other switching types described in IV-B, 76 cases of switching non-linear loads, 133 cases of switching lines, and 76 cases of simulations without any transients.

The results of the test using the five performance indexes mentioned previously are shown in Fig. 11. When trained on detailed data, the Proposed method utilizing the pretrained Squeezenet DNN outperformed the Method [20] employing LSTM in terms of all five parameters. When compared to the simplified ones, the two Detailed classifiers produced a significantly superior outcome. The results of these tests reveal that advanced pattern recognition techniques, in the absence of a robust database, yield inaccurate HIF detection methods. This is particularly evident when considering simulations with detailed DG models, which closely emulate real-world application scenarios. The methodology underperformed solely based on the security parameter when using simplified training data.

B. TESTS FOR HIF MODEL II

The ground surface material, surface humidity, feeder architecture, voltage levels, weather, and load type are just a few of the variables that have an impact on HIFs [3]. Therefore, creating a database from simulations that can accommodate all conceivable configurations of HIF occurrence in an MG is a highly challenging task. The tests with the HIF II and III models assess the resilience of the developed detection method. The idea is to subject the classifier to data from a HIF model not used during the training process and evaluate its performance.

The data set for training consists of 1050 cases (420 HIF, 630 nonHIF) and for testing are 570 cases (300 HIF, 270 nonHIF). The results are in Fig. 12. In order to create the test data set, all of the model II HIF data were removed from the training set and added to it.

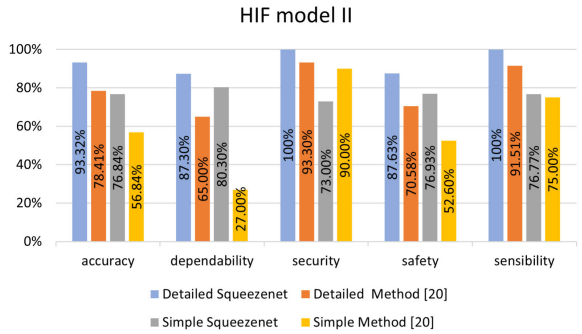

FIGURE 12. Classification performance for HIF model II.

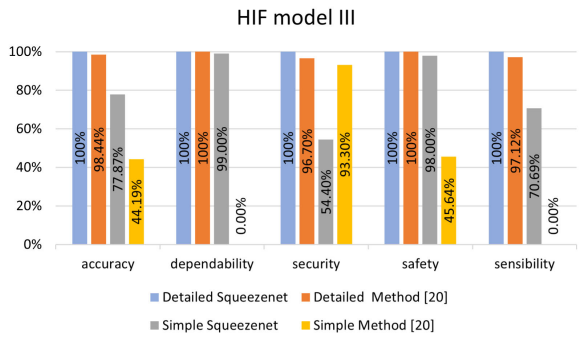

FIGURE 13. Classification performance for HIF model III.

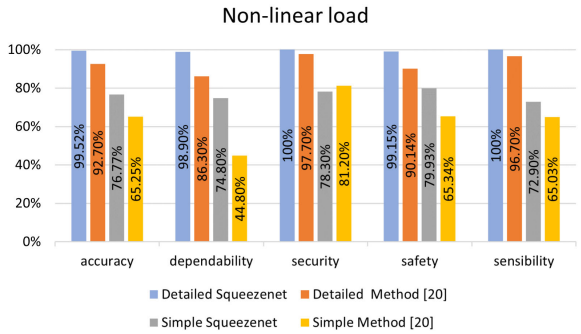

FIGURE 14. Classification performance for non-linear load.

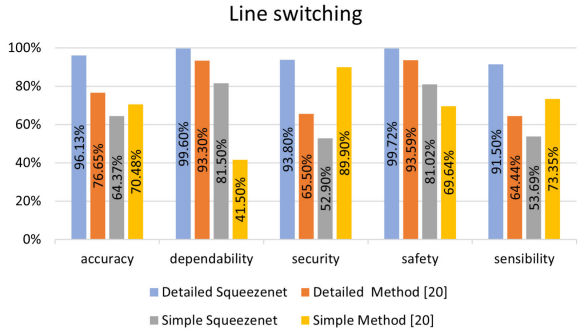

FIGURE 15. Classification performance for line switching.

Compared to the base case, the Detailed Squeezenet classifier maintained the safety and sensitivity indices, a small degradation in accuracy and a slightly lower performance than 90% in dependability and safety. The Detailed Method [20] classifier, on the other hand, showed a greater degradation in its performance indices, dropping from 93% to 78% in accuracy and from 89% to 65% in dependability. When compared to the base test using the entire database, the performance difference for Simple classifiers was not significant.

C. TESTS FOR HIF MODEL III

The same procedure used in the previous test was applied to evaluate HIF model III. The training data set consists of 1050 cases (210 HIF model I and 210 HIF model II, 630 nonHIF) and for testing 570 cases (300 HIF model III, 270 nonHIF). In this test, the detailed classifiers produced the best results, as seen in Fig. 13. The best accuracy for the Simple SqueezeNet classifier was achieved in this test.

As shown in Fig. 7, the resistors and DC sources in this HIF III model change randomly and independently every 0.1 ms. Despite this disparity from the other two HIF models, both Detailed classifiers were able to distinguish the characteristics of the HIF current signal in the scalogram images.

D. TESTS FOR NON-LINEAR LOAD CONNECTION

Non-linear loads have been previously mentioned in section II-D as having HIF-like features. Since these transients only arise in tests, the classifiers used in this test were not trained with them. There were 76 examples for training and 32 cases for testing in the first test, but all of them were only included in the test set here.

The two Detailed classifiers performed very similar to the first test, shown in Fig. 14. Thus, it is possible to confirm that non-linear load switching did not lead to misclassification despite sharing features with HIF. The simple classifiers obtained slightly better results compared to the first test, but due to their low performance, it is not feasible to use them in real applications.

E. TESTS FOR TRANSMISSION LINE SWITCHING

The purpose of this test is to verify whether changing MG arrangements after the closing or opening of the tie switch causes misclassification. Many HIF detection techniques consider radial distribution systems, which do not take into account this kind of scenario. The data sets for this test are 1027 cases (630 HIF 397 nonHIF) and for testing are 570 cases (270 HIF 403 nonHIF). The transmission line switching simulation data was all included in the test set and removed from the training set.

The evaluated indices produced the lowest scores for the Detailed Squeezenet classifier shown in Fig. 15. These rates, however, surpass the highest performance the Method [20] classifier could produce.

F. TESTS FOR NOISE RESILIENCE

To evaluate the performance of the Proposed Method in noisy environment, a white Gaussian noise of varying levels, (0 dB < SNR< 30 dB) was added to current signals in

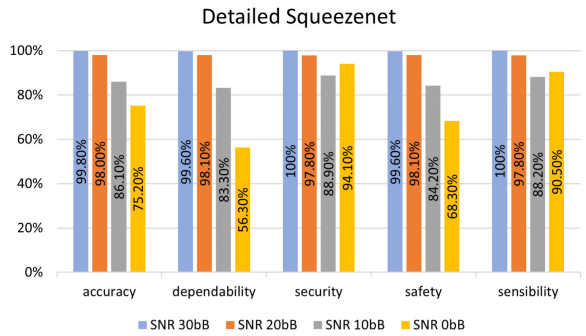

FIGURE 16. Detailed Squeezenet classification performance for the complete data set with noise.

test database. In the test, Detailed Squeezenet trained with complete database perform the classification on complete database for test, with performance shown in Fig. 16.

The classification method shows little degradation in performance for a signal-to-noise ratio (SNR) of 30 dB and 20 dB. For this level of noise the method presents performance, robustness and reliability consistent with real-world applications.

VI. CONCLUSION

In this paper, a new classifier is proposed for the problem of HIF detection in MGs. An emphasis is given to the impact of HIF modeling and DGs on classification performance when considering harmonic distortions caused by VSC based DG.

The simulations consider detailed models of DG and three different HIF models. The current measurements for all three phases are aggregated into a single time series by residual current calculation. The tested transient events were classified into HIF or nonHIF by a computationally sophisticated pattern recognition algorithm employing RGB images, which represent the time-frequency properties of the measured current signal. Five evaluation indexes, which represent a more comprehensive set of evaluation criteria, are employed to show the classification output.

To enhance the performance of HIF detection methods in MG, it is necessary to consider detailed simulation models, as suggested by the results. A harmonic distortion-free environment is not a realistic assumption for MG with VSC based DGs. Also, the HIF model should reproduce this phenomenon as accurately as possible in order to achieve good performance in real applications.

The results of the present study emphasize the need for using more accurate simulation models to improve the effectiveness of HIF identification. The accuracy of machine learning algorithms, in particular, is strongly influenced by the integrity of the training data, highlighting the critical role that high-quality data plays in achieving reliable and effective outcomes.

Two different HIF models and non-HIF transients were used in a series of five tests. For all of the evaluated conditions, the proposed classifier outperformed a recent HIF detection methodology, demonstrating its efficiency. The results demonstrated the robustness of the proposed methodology, indicating that neither overfitting nor underfitting occurred while detecting HIF from models for which it was not trained.

The noise resilience test was also performed. The results revealed adequate performance for systems with up to 20 dB SNR, demonstrating reliability for realistic fault scenarios. The increase in processing power and, with it, the development of new classification techniques are motivating factors for the proposition of more sophisticated and robust HIF detection methods, such as the one proposed in this paper.

The next stage of HIF detection technique development should consider more measurement points, a higher sample rate, and harmonic synchrophasor measurements. The detection method has the residual current as its input quantity. It has been verified that the approach is suitable for the cases considered. However, its applicability in other system topologies should be evaluated in future research, especially regarding the grounding scheme.

REFERENCES

[1] A. A. Bayod-Rújula, "Future development of the electricity systems with distributed generation," *Energy*, vol. 34, no. 3, pp. 377–383, Mar. 2009.

[2] S. Parhizi, H. Lotfi, A. Khodaei, and S. Bahramirad, "State of the art in research on microgrids: A review," *IEEE Access*, vol. 3, pp. 890–925, 2015.

[3] A. Ghaderi, H. L. Ginn, and H. A. Mohammadpour, "High impedance fault detection: A review," *Electric Power Syst. Res.*, vol. 143, pp. 376–388, Feb. 2017.

[4] M. Mishra and R. R. Panigrahi, "Taxonomy of high impedance fault detection algorithm," *Measurement*, vol. 148, Dec. 2019, Art. no. 106955.

[5] B. K. Chaitanya, A. Yadav, and M. Pazoki, "An intelligent detection of high-impedance faults for distribution lines integrated with distributed generators," *IEEE Syst. J.*, vol. 14, no. 1, pp. 870–879, Mar. 2020.

[6] P. K. Nayak, K. Sarwagya, and T. Biswal, "A novel high impedance fault detection technique in distribution systems with distributed generators," in *Proc. Nat. Power Syst. Conf. (NPSC)*, Dec. 2016, pp. 1–6.

[7] S. Gautam and S. M. Brahma, "Detection of high impedance fault in power distribution systems using mathematical morphology," *IEEE Trans. Power Syst.*, vol. 28, no. 2, pp. 1226–1234, May 2013.

[8] D. A. Gadanayak and R. K. Mallick, "Interharmonics based high impedance fault detection in distribution systems using maximum overlap wavelet packet transform and a modified empirical mode decomposition," *Int. J. Electr. Power Energy Syst.*, vol. 112, pp. 282–293, Nov. 2019.

[9] M. Biswal, M. Mishra, V. K. Sood, R. C. Bansal, and A. Y. Abdelaziz, "Savitzky-Golay filter integrated matrix pencil method to identify high impedance fault in a renewable penetrated distribution system," *Electric Power Syst. Res.*, vol. 210, Sep. 2022, Art. no. 108056.

[10] M. Bhatnagar, A. Yadav, and A. Swetapadma, "A resilient protection scheme for common shunt fault and high impedance fault in distribution lines using wavelet transform," *IEEE Syst. J.*, vol. 16, no. 4, pp. 5281–5292, Dec. 2022.

[11] M. Biswal, S. Ghore, O. P. Malik, and R. C. Bansal, "Development of time-frequency based approach to detect high impedance fault in an inverter interfaced distribution system," *IEEE Trans. Power Del.*, vol. 36, no. 6, pp. 3825–3833, Dec. 2021.

[12] M. Manohar, E. Koley, and S. Ghosh, "Microgrid protection against high impedance faults with robustness to harmonic intrusion and weather intermittency," *IET Renew. Power Gener.*, vol. 15, no. 11, pp. 2325–2339, Aug. 2021.

[13] D. R. R. Penido, L. R. de Araujo, V. T. S. Rodrigues, and K. B. do Nascimento, "An analytical zero sequence method to locate fault in distribution systems rich in DG," *IEEE Trans. Smart Grid*, vol. 13, no. 3, pp. 1849–1859, May 2022.

[14] M. Wei, W. Liu, H. Zhang, F. Shi, and W. Chen, "Distortion-based detection of high impedance fault in distribution systems," *IEEE Trans. Power Del.*, vol. 36, no. 3, pp. 1603–1618, Jun. 2021.

[15] A. Ahmadi, E. Aghajari, and M. Zangeneh, "High-impedance fault detection in power distribution grid systems based on support vector machine approach," *Electr. Eng.*, vol. 104, no. 5, pp. 3659–3672, Oct. 2022.

[16] F. Mumtaz, K. Imran, S. B. A. Bukhari, K. K. Mehmood, A. Abusorrah, M. A. Shah, and S. A. A. Kazmi, "A Kalman filter-based protection strategy for microgrids," *IEEE Access*, vol. 10, pp. 73243–73256, 2022.

[17] A. G. Rameshrao, E. Koley, and S. Ghosh, "A LSTM-based approach for detection of high impedance faults in hybrid microgrid with immunity against weather intermittency and N-1 contingency," *Renew. Energy*, vol. 198, pp. 75–90, Oct. 2022.

[18] É. M. Lima, R. D. A. Coelho, N. S. D. Brito, and B. A. D. Souza, "High impedance fault detection method for distribution networks under non-linear conditions," *Int. J. Electr. Power Energy Syst.*, vol. 131, Oct. 2021, Art. no. 107041.

[19] M. Wei, F. Shi, H. Zhang, and W. Chen, "Wideband synchronous measurement-based detection and location of high impedance fault for resonant distribution systems with integration of DERs," *IEEE Trans. Smart Grid*, vol. 14, no. 2, pp. 1117–1134, Mar. 2023.

[20] V. Veerasamy, N. I. A. Wahab, M. L. Othman, S. Padmanaban, K. Sekar, R. Ramachandran, H. Hizam, A. Vinayagam, and M. Z. Islam, "LSTM recurrent neural network classifier for high impedance fault detection in solar PV integrated power system," *IEEE Access*, vol. 9, pp. 32672–32687, 2021.

[21] S. Kar and S. R. Samantaray, "Time-frequency transform-based differential scheme for microgrid protection," *IET Gener., Transmiss. Distrib.*, vol. 8, no. 2, pp. 310–320, Feb. 2014. [Online]. Available: https://ietresearch.onlinelibrary.wiley.com/doi/abs/10.1049/iet-gtd.2013.0180

[22] S. Kar and S. R. Samantaray, "High impedance fault detection in microgrid using maximal overlapping discrete wavelet transform and decision tree," in *Proc. Int. Conf. Electr. Power Energy Syst. (ICEPES)*, Dec. 2016, pp. 258–263.

[23] M. Mishra and P. K. Rout, "Detection and classification of micro-grid faults based on HHT and machine learning techniques," *IET Gener., Transmiss. Distrib.*, vol. 12, no. 2, pp. 388–397, Jan. 2018.

[24] H. Laaksonen and P. Hovila, "Enhanced MV microgrid protection scheme for detecting high-impedance faults," in *Proc. IEEE Manchester PowerTech*, Jun. 2017, pp. 1–6.

[25] J. Deng, W. Dong, R. Socher, L.-J. Li, K. Li, and L. Fei-Fei, "ImageNet: A large-scale hierarchical image database," in *Proc. IEEE Conf. Comput. Vis. Pattern Recognit.*, Jun. 2009, pp. 248–255.

[26] A. A. Memon and K. Kauhaniemi, "A critical review of AC microgrid protection issues and available solutions," *Electric Power Syst. Res.*, vol. 129, pp. 23–31, Dec. 2015.

[27] A. Soheili, J. Sadeh, and R. Bakhshi, "Modified FFT based high impedance fault detection technique considering distribution non-linear loads: Simulation and experimental data analysis," *Int. J. Electr. Power Energy Syst.*, vol. 94, pp. 124–140, Jan. 2018. [Online]. Available: https://www.sciencedirect.com/science/article/pii/S0142061517306555

[28] Q.-M. Xiao, M.-F. Guo, and D.-Y. Chen, "High-impedance fault detection method based on one-dimensional variational prototyping-encoder for distribution networks," *IEEE Syst. J.*, vol. 16, no. 1, pp. 966–976, Mar. 2022.

[29] CIGRE Task Force C6.04.01. (2014). *Benchmark Systems for Network Integration of Renewable and Distributed Energy Resources*. CIGRE. [Online]. Available: http://www.e-cigre.org/Order/select.asp?ID=16639

[30] R. Azim, F. Li, Y. Xue, M. Starke, and H. Wang, "An islanding detection methodology combining decision trees and Sandia frequency shift for inverter-based distributed generations," *IET Gener., Transmiss. Distrib.*, vol. 11, no. 16, pp. 4104–4113, Nov. 2017. [Online]. Available: https://ietresearch.onlinelibrary.wiley.com/doi/abs/10.1049/iet-gtd.2016.1617

[31] A. Sultan and G. Swift, "Security testing of high impedance fault detectors," in *Proc. WESCANEX*, 1991, pp. 191–197.

[32] A. Soheili, J. Sadeh, H. Lomei, and K. Muttaqi, "A new high impedance fault detection scheme: Fourier based approach," in *Proc. IEEE Int. Conf. Power Syst. Technol. (POWERCON)*, Sep. 2016, pp. 1–6.

[33] A. E. Emanuel, D. Cyganski, J. A. Orr, S. Shiller, and E. M. Gulachenski, "High impedance fault arcing on sandy soil in 15 kV distribution feeders: Contributions to the evaluation of the low frequency spectrum," *IEEE Trans. Power Del.*, vol. 5, no. 2, pp. 676–686, Apr. 1990.

[34] Q. Cui, K. El-Arroudi, and G. Joos, "An effective feature extraction method in pattern recognition based high impedance fault detection," in *Proc. 19th Int. Conf. Intell. Syst. Appl. to Power Syst. (ISAP)*, Sep. 2017, pp. 1–6.

[35] T. M. Lai, L. A. Snider, E. Lo, and D. Sutanto, "High-impedance fault detection using discrete wavelet transform and frequency range and RMS conversion," *IEEE Trans. Power Del.*, vol. 20, no. 1, pp. 397–407, Jan. 2005.

[36] A. Aljohani and I. Habiballah, "High-impedance fault diagnosis: A review," *Energies*, vol. 13, no. 23, p. 6447, Dec. 2020. [Online]. Available: https://www.mdpi.com/1996-1073/13/23/6447

[37] A. R. Sedighi and M. R. Haghifam, "Simulation of high impedance ground fault in electrical power distribution systems," in *Proc. Int. Conf. Power Syst. Technol.*, Oct. 2010, pp. 1–7.

[38] A. Ghaderi, H. A. Mohammadpour, H. L. Ginn, and Y.-J. Shin, "High-impedance fault detection in the distribution network using the time-frequency-based algorithm," *IEEE Trans. Power Del.*, vol. 30, no. 3, pp. 1260–1268, Jun. 2015.

[39] M. Eslami, M. Jannati, and S. S. Tabatabaei, "An improved protection strategy based on PCC-SVM algorithm for identification of high impedance arcing fault in smart microgrids in the presence of distributed generation," *Measurement*, vol. 175, Apr. 2021, Art. no. 109149. [Online]. Available: https://www.sciencedirect.com/science/article/pii/S0263224121001731

[40] S. J. Pan and Q. Yang, "A survey on transfer learning," *IEEE Trans. Knowl. Data Eng.*, vol. 22, no. 10, pp. 1345–1359, Jan. 2009.

[41] F. N. Iandola, S. Han, M. W. Moskewicz, K. Ashraf, W. J. Dally, and K. Keutzer, "SqueezeNet: AlexNet-level accuracy with 50x fewer parameters and <0.5 MB model size," 2016, *arXiv:1602.07360*.

[42] Y. Zhang, X. Wang, J. He, Y. Xu, F. Zhang, and Y. Luo, "A transfer learning-based high impedance fault detection method under a cloud-edge collaboration framework," *IEEE Access*, vol. 8, pp. 165099–165110, 2020.

[43] Y. Zhang, X. Wang, Y. Luo, Y. Xu, J. He, and G. Wu, "A CNN based transfer learning method for high impedance fault detection," in *Proc. IEEE Power Energy Soc. Gen. Meeting (PESGM)*, Aug. 2020, pp. 1–5.

[44] R. Fan and T. Yin, "Convolutional neural network and transfer learning for high impedance fault detection," 2019, *arXiv:1904.08863*.

VITOR FERNANDO COUTO received the B.E. and M.E. degrees in electrical engineering (power systems) from the Regional University of Blumenau, Brazil, in 2011 and 2013, respectively. He is currently pursuing the Ph.D. degree in electrical engineering with the Federal University of Santa Catarina, Florianópolis, Brazil. He is an Innovation Researcher with the WEG Group. His research interests include pattern recognition, signal processing, and artificial intelligence for fault identification in electrical power systems.

MIGUEL MORETO received the B.Sc. and M.Sc. degrees in electrical engineering from the Federal University of Rio Grande do Sul, Porto Alegre, Brazil, in 2003 and 2005, respectively, and the D.Sc. degree in electrical engineering from the Federal University of Santa Catarina, Florianópolis, Brazil, in 2011. He is currently an Adjunct Professor with the Federal University of Santa Catarina. His research interests include computational intelligence applications to power systems, disturbance diagnosis, protection systems, and power systems signal processing and synchrophasor measurements in distribution systems.